INTERNATIONAL JOURNAL FOR NUMERICAL METHODS IN FLUIDS
Int. J. Numer. Meth. Fluids 2004; **45**:391–419 (DOI: 10.1002/fld.704)

Influence of inertia, topography and gravity on transient axisymmetric thin-film flow

Roger E. Khayat[1,*,†], Kyu-Tae Kim[1] and Steven Delosquer[2]

[1]*Department of Mechanical and Materials Engineering, University of Western Ontario, London, Ontario, Canada N6A 5B9*
[2]*Laboratoire de Mécanique et Matériaux, École Centrale de Nantes, BP 92101, Nantes 44321, Cédex 3, France*

SUMMARY

This study examines theoretically the development of early transients for axisymmetric flow of a thin film over a stationary cylindrical substrate of arbitrary shape. The fluid is assumed to emerge from an annular tube as it is driven by a pressure gradient maintained inside the annulus, and/or by gravity in the axial direction. The interplay between inertia, annulus aspect ratio, substrate topography and gravity is particularly emphasized. Initial conditions are found to have a drastic effect on the ensuing flow. The flow is governed by the thin-film equations of the 'boundary-layer' type, which are solved by expanding the flow field in terms of orthonormal modes in the radial direction. The formulation is validated upon comparison with the similarity solution of Watson (*J. Fluid Mech* 1964; **20**:481) leading to an excellent agreement when only 2–3 modes are included. The wave and flow structure are examined for high and low inertia. It is found that low-inertia fluids tend to accumulate near the annulus exit, exhibiting a standing wave that grows with time. This behaviour clearly illustrates the difficulty faced with coating high-viscosity fluids. The annulus aspect is found to be influential only when inertia is significant; there is less flow resistance for a film over a cylinder of smaller diameter. For high inertia, the free surface evolves similarly to two-dimensional flow. The substrate topography is found to have a significant effect on transient behaviour, but this effect depends strongly on inertia. It is observed that the flow of a high-inertia fluid over a step-down exhibits the formation of a secondary wave that moves upstream of the primary wave. Gravity is found to help the film (coating) flow by halting or prohibiting the wave growth. The initial film profile and velocity distribution dictate whether the fluid will flow downstream or accumulate near the annulus exit. Copyright © 2004 John Wiley & Sons, Ltd.

KEY WORDS: thin film; axisymmetric flow; gravity; inertia; unified spectral approach

1. INTRODUCTION

This study focuses on the influence of inertia, annulus aspect ratio, substrate topography and gravity during the early stages of flow development of a fluid film emerging from an

*Correspondence to: Roger E. Khayat, Department of Mechanical and Materials Engineering, University of Western Ontario, London, Ontario, Canada N6A 5B9.
†E-mail: rkhayat@eng.uwo.ca

Contract/grant sponsor: Natural Sciences and Engineering Research Council of Canada

Received 14 April 2003
Revised 13 October 2003

annular duct (die), and flowing on a solid and stationary axisymmetric substrate of arbitrary shape. The evolution of thin-film flow involves typically three distinct stages that are usually identified after flow inception. The first stage is the formation of a wave and its propagation near the source, the second is the free propagation of the wave on the open substrate and the third is the development of the steady-state flow that will finally lead to the formation of the steady (but not necessarily uniform) film thickness. In this study, the modelling and simulation of the three stages are performed for axisymmetric flow in order to examine the intricate wave and flow structures that develop. The problem thus consists of obtaining the shape of the evolving free surface and the flow field inside the moving domain, as the fluid emerges from the annulus. The flow is induced by the pressure gradient inside the annulus, where fully developed Poiseuille conditions are assumed to prevail, and/or gravity in the axial direction.

Generally, most studies on thin-film flow involve either gravity- or surface-tension-driven flow, or both [1–6]. Rarely is pressure-driven flow contemplated. The flow of a falling film on an inclined or vertical wall has been extensively investigated [2, 7–12]. Some studies on surface-tension-driven flows include [5, 13]. Although the literature abounds with two-dimensional studies, other geometries have also been considered. In particular, axisymmetric flows have been examined, including radial spreading [14], spin coating [3, 11, 13, 15–17], and flow over a cylinder [18–20]. Most of the theoretical work has concentrated on Newtonian fluids, and, to a much lesser extent, on non-Newtonian fluids [15, 21–25]. The effect of other external (body) forces has also been considered. Gorla and Byrd examined the effect of an electrostatic field on the flow of a film, its stability, and eventual rupture [26]. The action of an external air jet on thin films was considered [16, 27–29].

The effect of substrate topography was recently considered by Kalliadasis *et al.* on the steady thin-film flow over trenches and mounds [30]. Their study was limited, however, to surface-tension dominated inertialess flow. They found that the free surface develops a ridge right before the entrance to the trench or exit from the mound, and that the ridge can become large for steep substrate features of significant depth. Earlier, Stillwagon and Larson investigated this problem experimentally [31]. They measured the changes in thickness of silicon oil films at the centre of holes and trenches of a silicon substrate using a non-contact interferometric technique. In that case, the flow was also surface-tension dominated, and inertia effect was negligible. Later, Stillwagon and Larson considered the levelling of thin films over uneven substrates during spin coating [32]. This problem was also considered by Spaid and Homsy for an Oldroyd-B fluid [15]. More recently, Ruschak and Weinstein examined the gravity-driven flow of a thin film over a round-crested weir [33]. Similarly to the present problem, surface-tension effect was neglected, and inertia effect was included. The equations were depth averaged in the radial direction. Steady-state profiles of the free surface were obtained as function of the Reynolds number and weir diameter. Duffy and Wilson used the lubrication approximation to examine the steady two-dimensional flow on the outside of a rigid circular rotating cylinder. Inertia as well as surface-tension effects were neglected [34].

Transient flow studies are often limited to the linear destabilization of the film or to small-amplitude motion [1, 8, 23]. Studies on finite-amplitude film deformation include the spreading in spin coating [13, 16], the evaporation of liquid films [35], the deformation of long vapour bubbles due to the evaporation from the surrounding liquid [36], the instability and breakup of long annular liquid layers [19, 20], evolution of a falling film [2, 3, 10, 12, 18, 29, 37, 38]. Of closer relevance to the present problem, is the simulation of Kalliadasis and Chang, who

examined the critical conditions for the formation of solitary waves during the coating of vertical fibres [18]. The long-wave equation was solved using a matched asymptotic expansion, which joins the capillary outer region of the large solitary wave to the thin-film inner region. Inertia was neglected. Nguyen and Balakotaiah proposed an integral boundary-layer model for a free falling film [12].

The interplay between inertia and other forces in thin-film flow has been examined in the literature. Szeri reviewed some of the attempts made to extend the classical Reynolds equation to include the effect of fluid inertia in lubrication theory [21]. In a review article on fibre coating, Quéré discussed the effect of inertia on rapid coating and droplet expulsion [39]. Tuck and Bentwich determined the steady two-dimensional flow between sliding sheets at finite Reynolds number [40]. The flow was obtained approximately on the basis of an *ad hoc* linearization of the convective term. More recently, a similar approximation was used by Wilson and Duffy, who examined the effect of inertia for a fluid flowing in a channel of arbitrary cross section [34]. Earlier, Watson examined the steady laminar and turbulent radial spread of a liquid jet over a horizontal plane, including the special case of two-dimensional flow [14]. For a large distance from the source, a similarity solution of the laminar boundary-layer equations was sought. In particular, Watson found that for two-dimensional flow, the steady (dimensionless) shape of the free surface is given by $\eta_s = \pi x/\sqrt{3}\,Re = 1.81x/Re$, where x is the distance from the source, and Re is the (modified) Reynolds number. The steady surface profile was obtained in the absence of gravity and surface tension. It constitutes an important limit form, which will be compared against the present formulation. Khayat and Welke examined the two-dimensional transient film flow [41]. Comparison with Watson's similarity solution led to good agreement.

Although the thin-film formulation reduces the pressure to its hydrostatic part, thus eliminating the momentum equation in the transverse (vertical or radial) direction from the problem, the dimension of the problem remains the same as the original equations. Benney's long-wave (LW) approximation is often used [42], especially for small-inertia flow. At high Reynolds number, inertia is better accounted for through the 'boundary-layer' (BL) approximation, which includes the effect of transverse flow. Salamon *et al.* carried out a finite element solution of the full Navier–Stokes equations for the flow in a falling film [43]. Comparison of their results with those based on the LW approximation, indicates that serious limitations exist in the validity of the LW equation. The major difference between the original Navier–Stokes equations and the BL equations is the hydrostatic variation of the pressure across the film depth. As a result, only the transverse momentum equation is eliminated, but the convective terms are retained in the remaining equations, and the number of boundary conditions is reduced. However, the solution of the BL equations remains essentially as difficult to obtain as that of the Navier–Stokes equations [38]. A depthwise integration of the momentum equation(s) in the lateral direction(s) is usually performed by assuming a self-similar semi-parabolic flow profile in the transverse direction, as was proposed [44]. Although the depth-averaged equations are only of second order in time, they yield plausible results, at least qualitatively, but they remain fundamentally questionable because of the semi-parabolic assumption [8, 38]. A measure of the error involved may be inferred by computing the free-surface profile in the absence of gravity and surface tension, and comparing it to Watson's result given above. From the literature, the steady-state profile based on the semi-parabolic profile is easily found to be $\eta_s = 2.5x/Re$ [2]. The parabolic approximation is widely used in the literature, and its validity was established experimentally by Alekseenko *et al.* [7].

However, it is generally argued that the parabolic approximation is valid at low or moderately low Reynolds number, and provided the waves are far from the entry [45, 46]. In addition to high-inertia flow, other flow conditions that restrict the range of validity of the semi-parabolic profile include the presence of end effects, turbulent flow and (most likely) non-linear effects stemming from shear-thinning or viscoelastic effects [47]. A more rigorous approach for the solution of the thin-film equations becomes almost as difficult to achieve as for the original Navier–Stokes equations. Hence, conventional solution techniques such as the finite element or finite difference methods are not suitable given the rapid spatio-temporal variation of the flow field in the presence of steep waves. Frequent remeshing, and an effective implicit time-stepping scheme are required. Ruyer–Quil and Manneville used a three-term expansion of the flow field in the transverse direction, and obtained three coupled equations for the surface height, flow rate and stress [11]. Takeshi examined the flow in a falling film at moderate Reynolds number and large but finite Weber number, using a regularization method, which consists of a combination of the Padé approximation and the long-wave expansion [38].

In this study, a unified spectral approach is proposed to model the pressure- and/or gravity-driven axisymmetric flow of a thin film over a substrate of arbitrary shape. Given the importance of inertia upon inception, the BL formulation rather than Benney's LW approximation [42] will be used. The flow equations are first mapped over the rectangular domain, and a formal expansion of the velocity field in terms of orthonormal basis functions is introduced for the flow field. The formulation closely follows and generalizes that of Zienkiewicz and Heinrich, which emphasizes water flow over extended areas [48]. There are, however, three major simplifying assumptions adopted by Zienkiewicz and Heinrich [48], which will be relaxed in the present study. First, the radial (transverse) velocity component will not be neglected in the momentum equation. Second, despite the long-wave approximation, the variation in surface height will not be neglected with respect to time and space in the momentum equation. Third, a spectral approach is proposed, whereby the flow field is expanded in terms of mixed trigonometric/hyperbolic orthonormal functions, instead of simple polynomials, to represent the flow in the transverse direction. The Galerkin projection method is used to generate the equations that govern the expansion coefficients. A Lagrangian time-stepping implicit finite difference approach is implemented for the solution of the equations that govern the expansion coefficients, coupled with a Runge–Kutta integration scheme along the flow direction. The spectral method, and, particularly, the low-dimensional description of flow, has emerged as an effective alternative to conventional methods [49]. Although this method has predominantly been used for simple flow, recent developments have included complex geometry [50], and complex fluids [51–53].

Unlike the depth-averaging method, the proposed spectral methodology becomes particularly suited for the early onset of wave motion near the annulus exit. Assessment of convergence and accuracy is carried out by adopting different truncation levels, varying the time increment and mesh size and monitoring the conservation of mass (volume). The overall validity of the basic approach is established by comparing the two-dimensional steady-state solution against the similarity solution of Watson [14], and the solution based on the parabolic profile and the depth-averaging procedure [2]. The problem thus consists of obtaining the shape of the evolving free surface and the flow velocity inside a moving domain, as the fluid emerges from the annulus. The flow is induced by the pressure gradient inside the annulus, where fully developed Poiseuille conditions are assumed to prevail. The study emphasizes the influence

of inertia and substrate topography. Details of the free surface and flow field can be captured explicitly and in the mean sense.

The paper is organized as follows. The problem formulation and solution procedure are given, respectively, in Section 2. Numerical assessment and results are presented in Section 3, with detailed account of the effects of inertia, annulus aspect ratio, substrate topography and gravity on transient flow behaviour and wave formation. Finally, discussion and concluding remarks are given in Section 4.

2. PROBLEM FORMULATION AND SOLUTION PROCEDURE

The general formulation is implemented for the problem of transient axisymmetric flow of a fluid over a rigid surface as depicted in Figure 1. The equations and boundary conditions are deduced for a flow driven by an imposing pressure at the exit of the annulus.

2.1. Thin-film equations and boundary conditions

Consider the flow of an incompressible fluid of density ρ, and viscosity μ, emerging from an annulus as depicted from Figure 1. Note that the X-axis is directed vertically downward. Surface-tension effect is assumed to be negligible. The flow may be induced by a pressure gradient inside the annulus (Poiseuille flow) or simply by gravity. The emphasis in this study, however, is on the former configuration. Let T be the time. The fluid is assumed to occupy a domain $\Omega(T)$, which is bounded by the free surface $\Gamma_F(T)$, the wetted part of the cylindrical substrate, Γ_W and the annulus exit Γ_E. Since the flow is axisymmetric, it will be examined in the (X,R)-plane, with $R=0$ coinciding with the axis of the cylindrical substrate. The shape of the substrate is given by $R=R_S(X)$. The velocity components and pressure are denoted by (U_X, U_R) and P, respectively. The free-surface height is given by $R=E(X,T)$. The reference thickness, H, is taken as $H=E(X=0,T)-R_S(X=0)$, where $X=0$ coincides with the annulus exit. The reference length is taken as $R_{S0}=R_S(X=0)$. Similarly to two-dimensional thin-film theory, the dimensionless variables are introduced as follows:

$$x=\frac{X}{R_{S0}}, \quad z=\frac{R-R_{S0}}{H}, \quad t=\frac{V}{R_{S0}}T, \quad u=\frac{U_x}{V}$$
$$w=\frac{R_{S0}U_R}{VH}, \quad p=\frac{H^2}{\mu V R_{S0}}P, \quad h=\frac{R_S-R_{S0}}{H}, \quad \eta=\frac{E-R_{S0}}{H} \tag{1}$$

where V is a reference velocity, which will be taken as the mean flow velocity of the fluid inside the annulus. Here (u,w) are the velocity components in the (x,z) plane. The (dimensionless) shape of the free surface is then given by $z=\eta(x,t)$, and that of the substrate by $z=h(x)$. The scaling for the pressure is chosen to ensure the balance between pressure and viscous forces [5].

There are three important dimensionless groups that emerge in the formulation, namely, the Reynolds number, Re, the aspect ratio, ε, at the annulus exit and the Froude number:

$$Re=\frac{VH^2}{\nu R_{S0}}, \quad \varepsilon=\frac{H}{R_{S0}}, \quad Fr=\frac{V}{\sqrt{gR_{S0}}} \tag{2}$$

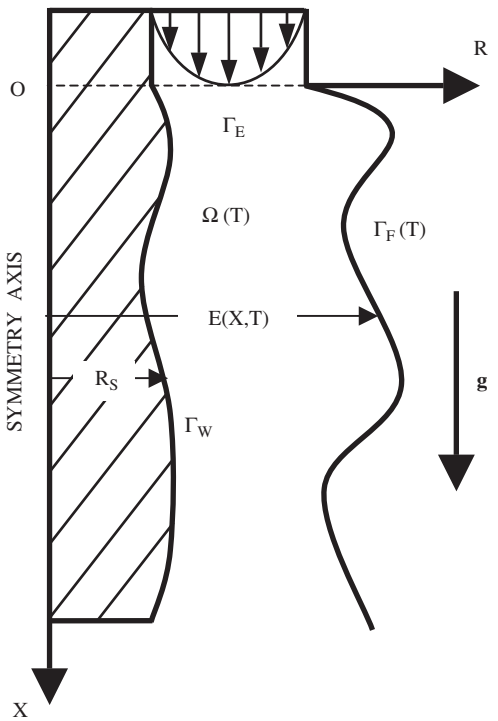

Figure 1. Schematic illustration of the axisymmetric flow emerging from an annulus. The figure also shows the dimensionless notations used in the formulation.

where v is the kinematic viscosity. Following Frenkel [60], the Navier–Stokes equations are cast in dimensionless form, and terms of $O(\varepsilon^2)$ and higher are excluded. In this case, the radial momentum equation simply states that the pressure is reduced to its hydrostatic part. Since there is no body force acting in the radial direction, then $p = p(x,t)$. It is also assumed that no (wind) pressure acts on the fluid surface; see, for instance, Kriegsmann *et al.* who examined pressure-driven flow [54]. The conservation of mass and momentum reduce, respectively, to

$$u_x + \varepsilon w + w_z = 0 \tag{3}$$

$$Re(u_t + uu_x + wu_z) = u_{zz} + \varepsilon u_z + \frac{Re}{Fr^2} \tag{4}$$

where a subscript x, z or t denotes partial differentiation.

The evolution of the free surface is dictated by the kinematic condition:

$$w(x, z = \eta, t) = \eta_t(x,t) + u(x, z = \eta, t)\eta_x(x,t) \tag{5}$$

The dynamic condition at the free surface reduces to following conditions when terms of $O(\varepsilon^2)$ and higher are excluded:

$$u_z(x, z = \eta, t) = 0 \tag{6}$$

The no-slip boundary condition at the substrate gives

$$u(x, z = h, t) = w(x, z = h, t) = 0 \tag{7}$$

The boundary conditions at the die exit ($x = 0$), as well as the initial conditions will be given below.

Equations (3) and (4) are of the 'boundary-layer' type, which must be solved subject to conditions (5)–(7) in the z direction. If ε is set equal to zero, the problem reduces to that corresponding to two-dimensional film flow [2, 3]. *Re* is sometime referred to as the modified Reynolds number [55], which is expressed in terms of the Reynolds number based on R_{S0} or $Re = \varepsilon^2(VR_{S0}/\nu)$. Although *Re* may be small for most polymeric flows, it may be large for other fluids such as liquid metals. In this work, inertia effects will be included to cover the widest possible range of flows. In the absence of inertia, the axial velocity component is determined by simply integrating Equation (4) with respect to z, and applying the boundary conditions. One thus recovers the parabolic and cubic profiles similarly to fully developed flow between two concentric cylinders. In this case, the transverse component of velocity, w, is not needed, although it can be obtained by integrating Equation (3). In contrast, when inertia effects are included, the transverse velocity is no longer decoupled between the continuity and the axial momentum equations. Similarly to u, w becomes an unknown in the problem. Note that the pressure is no longer an unknown in the problem, since it vanishes everywhere and at all time. Equations (3) and (4) become the two governing equations for the two velocity components.

Regarding the effect of surface tension, an axisymmetric fluid film is expected to destabilize, exhibiting spontaneous undulation, to finally break into a periodic array of droplets [56]. However, instability is not expected when the film thickness is small. Equivalently, as Plateau showed, only axisymmetric wavelengths larger than the circumference $2\pi E$ (see Figure 1) are unstable [57]. Frenkel, Babchin, Levich, Shlang and Sivashinsky showed that gravity-driven flow can keep the film from rupturing (in the form of droplets) as a result of the non-linear saturation of the instability, which is generated by the coupling between instability growth and the driving force (gravity or pressure as in the present problem) [58]. Quéré examined experimentally the conditions for instability of film flow down fibres (under gravity). He found that the film thickness must reach a critical value that is proportional to the cube of the fibre radius for instability to occur (see in Reference [7, *Equation*(4)]). In dimensionless terms, the film remains stable for $\varepsilon^3 \mathrm{Ca} < 1.4Re$, where $\sqrt{gR_{S0}}$ is taken as the velocity scale. The inequality also corresponds to a growth time of instability that is smaller than the convection time. In other words, destabilization does not occur when inertia is significant, the film is thin and/or surface tension effect is small. A similar criterion is expected to hold for pressure-driven flow. Later, Frenkel confirmed Quéré's criterion and found it not to depend on fluid viscosity [59]. Thus, according to Frenkel, non-linear convective effects are the ones responsible for the saturation of Rayleigh instability. The saturation mechanism is further interpreted by Kalliadasis and Chang, where a detailed numerical study of film evolution can be found [18].

2.2. Solution procedure

Given the small thickness of the film, the governing equations are usually depth-averaged across the thickness. This step is justified on the basis that the flow field should not vary significantly in the z direction. The presence of the non-linear convective terms in Equation (4)

do not allow an exact averaging process. The key difficulty, of course, is the explicit z dependence of the velocity components. Even if the x and z dependencies can be assumed to be decoupled, with a separation of variables-type argument becoming possible, the question remains as to the type of z dependence that u and w must have. Several types and levels of approximations have been used in the literature, the most prominent of which being the assumption of a similarity semi-parabolic profile [8, 14, 44]. Expectedly, the similarity profile loses its validity when inertia is important. In this case, more formal treatments in the form of flow expansions in the z direction were suggested [11, 38, 48].

In this paper, the flow field is expanded in terms of appropriately chosen modes in the z direction, and the Galerkin projection method is applied to generate the equations that govern the expansion coefficients. The procedure is closely related to but generalizes the formulation of Zienkiewicz an Heinrich [48] for the flow of a thin film, and includes the depth-averaging scheme as a limit case. In particular, it is assumed that u can be represented by a contribution of some basic shape functions, $\phi_i(\xi)$, such that

$$u(x,z,t) = \sum_{i=1}^{M} U_i(x,t)\phi_i(\xi) \tag{8}$$

where M is the number of modes, $U_i(x,t)$ are the unknown expansion coefficients, and $\xi = 1/(\eta - h)[z - (\eta + h)/2]$ is the transformation from $z \in [h,\eta]$ to $\xi \in [-1/2, +1/2]$. Conditions (6) and (7) impose the following restrictions on the shape functions:

$$\phi_i'(\xi = +1/2) = \phi_i(\xi = -1/2) = 0, \quad \forall i \in [1,\ M] \tag{9}$$

where a prime denotes differentiation with respect to ξ. The mean flow across the depth, $U(x,t)$, is given by

$$U(x,t) = \frac{1}{\Delta}\int_h^\eta (1+\varepsilon z)u\,\mathrm{d}z = \sum_{i=1}^{M} U_i \left\langle \phi_i \left(1 + \frac{\varepsilon\Sigma}{2} + \varepsilon\Delta\xi\right)\right\rangle \tag{10}$$

where $\Delta(x,t) = \eta(x,t) - h(x)$, $\Sigma(x,t) = \eta(x,t) + h(x)$, and $\langle\rangle$ denotes the integral over $\xi \in [-1/2, +1/2]$. Note that the flow rate is given by $Q = U(\eta - h)$.

The shape functions are chosen to satisfy conditions (9) and the two-dimensional flow limit ($\varepsilon = 0$). In two-dimensional flow, the leading shape function is taken to be parabolic in z, in analogy to channel Poiseuille flow [2, 26, 33]. However, in the present problem, and in analogy to pressure-driven flow between two concentric cylinders, two leading modes are needed, one is parabolic and the other cubic. Without loss of generality, the shape functions are taken to satisfy the following properties:

$$\langle\phi_1\rangle = 1, \quad \langle\phi_{i>1}\rangle = 0 \tag{11}$$

where ϕ_1 is parabolic and ϕ_2 is cubic in ξ. In this case, $\phi_1 = -(\xi^2 - \xi - 3/4)/6$ and $\phi_2 = 8\xi^3 - 3\xi^2/ - 3\xi + 1/4$. The remaining modes $\phi_{i>2}$ are taken as orthonormal odd functions of the Chandrasekhar type [60]. It is important to observe that, in the absence of inertia, the exact solution is recovered through the two leading-order modes for axisymmetric flow, and the leading-order mode for two- dimensional flow.

The radial velocity component is obtained by integrating Equation (3) over the interval $[h,z]$, to provide

$$w(x,z,t) = -\Delta \sum_{i=1}^{M} [(1-\varepsilon\Delta\xi)F_i + \varepsilon\Delta G_i]U_{i_x} + \sum_{i=1}^{M} \left[\left(\frac{\Sigma_x}{2} + \Delta_x \xi \right) \phi_i + \left(\varepsilon\Delta\Delta_x \xi - \Delta_x - \varepsilon\Delta \frac{\Sigma_x}{2} \right) F_i - 2\varepsilon\Delta\Delta_x G_i \right] U_i \tag{12}$$

where $F_i(\tau) = \int_{-1/2}^{\tau} \phi_i(\tau)\,\mathrm{d}\tau$ and $G_i(\tau) = \int_{-1/2}^{\tau} \tau\phi_i(\tau)\,\mathrm{d}\tau$.

The mean radial velocity is easily determined from Equation (12), which is here introduced as

$$W(x,t) = \frac{1}{\Delta} \int_h^{\eta} (1+\varepsilon z) w \,\mathrm{d}z$$

The evolution of the free surface is dictated by an equation that can be obtained by integrating the continuity equation (3) over the interval $z \in [h,\eta]$. Upon applying Leibnitz's rule and using expressions (7)–(10), the kinematic condition (5) becomes

$$(1+\varepsilon\eta)\eta_t = -(\eta_x - h_x)U - (\eta - h)U_x = -\Delta_x U - \Delta U_x \tag{13}$$

It is argued that any arbitrary number of modes can be introduced, each satisfying conditions (9) and (11), but reasonable radial distributions can be obtained with $M = 2$ or 3 for most practical applications [48]. More importantly, since the aim of the present study is to examine the influence of inertia and substrate topography, higher-order modes will only lead to a slightly better accuracy, without changing the qualitative picture. These observations will be confirmed below when convergence and accuracy are assessed. Of course, the rate of convergence will strongly depend on the choice of the modes. In addition, given the small thickness of the fluid film, the flow field is not expected to vary strongly with the height z.

An hierarchy of equations are obtained for the coefficients $U_i(x,t)$, when expression (8) is substituted into the momentum equation (4), which is then multiplied by $\phi_{i\geqslant 1}$ and integrated over $\xi \in [-1/2, +1/2]$. If w is eliminated by using (12), then one has

$$\begin{aligned} &\sum_{j=1}^{M} \left[\langle \phi_i \phi_j \rangle U_{j_t} - \frac{\eta_t}{\Delta} \left(\xi + \frac{1}{2} \right) \langle \phi_i \phi_j' \rangle U_j \right] \\ &\quad + \sum_{j=1}^{M} \sum_{k=1}^{M} \left\{ [\langle \phi_i (\phi_j \phi_k - \phi_j' F_k) \rangle - \varepsilon\Delta \langle \phi_i \phi_j' (G_k - \xi F_k) \rangle] - U_j U_{k_x} \right. \\ &\quad \left. + \left[\varepsilon\Delta_x \langle \phi_i (\xi F_j - 2G_j) \phi_k' \rangle - \left(\frac{\Delta_x}{\Delta} + \varepsilon \frac{\Sigma_x}{2} \right) \langle \phi_i F_j \phi_k' \rangle \right] U_j U_k \right\} \\ &\quad = \frac{1}{\Delta Re} \sum_{j=1}^{M} \left[\varepsilon \langle \phi_i \phi_j' \rangle + \frac{1}{\Delta} \langle \phi_i \phi_j'' \rangle \right] U_j + \frac{\langle \phi_i \rangle}{Fr^2}. \end{aligned} \tag{14}$$

The problem is completed by imposing boundary and initial conditions on $U_i(x,t)$. The free-surface height and mean velocity (flow rate) are imposed at the annulus exit. In this study,

the fluid is assumed to emerge at a normalized flow rate, $U(x=0,t)=1$, and is assumed to always adhere to the outer cylinder at the exit, so that

$$\eta(x=0,t)=1, \quad U_1(x=0,t)=\frac{8}{8+5\varepsilon}, \quad U_{i>1}(x=0,t)=0 \tag{15}$$

where $h(x=0)=0$ is used. The initial conditions may generally be written as

$$\eta(x,t=0)=\eta_0(x), \quad U_1(x,t=0)=U_0(x), \quad U_{i>1}(x,t=0)=0 \tag{16}$$

which will be specified once a particular problem is solved. Note that $\eta_0(0)=1$ and $U_0(0)=8/(8+5\varepsilon)$. The solution of system (13) and (14), subject to conditions (15) and (16), is obtained by using an implicit forward finite difference scheme in time, combined with a sixth-order Runge–Kutta integration in space. It is particularly convenient in this case to treat η_x explicitly in Equation (14).

Although the study focuses mainly on the development of early transient flow, it is useful to examine the steady-state problem for reference. Some limit flows are now considered. In particular, a relation between the steady-state mean component, $U_{S(x)}=U(x,t\to\infty)$, and the free-surface height, $\eta_S(x)\equiv(x,t\to\infty)$, is readily obtained by integrating Equation (13) which, upon applying conditions (15), reads

$$\eta_s(x)=\frac{1}{U_s(x)}+h(x) \tag{17}$$

The expansion coefficients for the velocity are then obtained by solving Equation (14), with the transient terms set equal to zero, as a set of ordinary differential equations in x. Another quantity of interest is the steady-state radial velocity component, $W_S(x)\equiv W(x,t\to\infty)$, which will also be examined. In general, that is, for an arbitrary number of modes and variable topography, the steady-state solution is difficult to obtain analytically. However, some progress can be made for two-dimensional flow, and the result can be compared to that Watson [14].

2.3. *Two-dimensional flow limits*

Upon setting $\varepsilon=0$, the formulation for two-dimensional flow can be recovered. Analytical solutions can be obtained for some limit flows. It will be demonstrated in the next section that the flow behaviour is essentially uninfluenced by higher-order modes. For axisymmetric flow, the two leading modes, $U_1(x,t)$ and $U_2(x,t)$, are found to be by far the most dominant modes. In two dimensions, $U_1(x,t)$ becomes the most dominant mode. If $U_{i>1}(x,t)$ and ε are set equal to zero, one obtains a generalization of the depth-averaged equation for the mean velocity, which reads

$$C_1U_t-\frac{\eta_t}{\Delta}C_2U+C_3UU_x-\frac{\Delta_x}{\Delta}C_4U^2=\frac{C_5}{\Delta^2Re}U+\frac{1}{Fr^2} \tag{18}$$

where $C_1=\langle\phi_1^2\rangle$, $C_2=\langle\xi\phi_1\phi_1'\rangle+0.5\langle\phi_1\phi_1'\rangle$, $C_3=\langle\phi_1^3\rangle-\langle\phi_1F_1\phi_1'\rangle$, $C_4=\langle\phi_1F_1\phi_1'\rangle$ and $C_5=\langle\phi_1\phi_1''\rangle$. Note that in this case, the mean vertical velocity component, $W(x,t)$, is obtained by integrating expression (12). The steady-state solution must be determined numerically. However, if h is assumed to be independent of x, and therefore $h=1$, then the steady-state velocity coefficient and free-surface height can be obtained explicitly. If, further, gravity effect is neglected, the solution can be compared to Watson's [14]. Thus, in the limit $Fr\to\infty$, the

steady-state solution of Equation (18) leads, to the following expressions for the mean velocity and free surface:

$$U_s(x) = \frac{Re}{Re + Cx}, \quad \eta_s(x) = \frac{C}{Re}x + 1 \tag{19}$$

where $C = -C_5/(C_3 + C_4) = 1.944$. The solution including gravity effect will be considered in some detail below. Solutions (19) show that, at finite Reynolds number, the velocity decreases from 1 at the annulus exit, and behaves like Re/x for large x, and the free surface increases linearly with x. In the limit $Re \to \infty$, $U_S \to 1$, and $\eta_S \to 1$. In the limit $Re \to 0$, $U_S \to 0$, and the free surface becomes singular, behaving like $1/Re$. Thus, low-inertia fluids tend to emerge from the annulus with a sudden expansion. This important conclusion also holds for axisymmetric flow, and will be confirmed in Section 3 when numerical results are presented, in the presence and absence of gravity.

Expressions (19) are comparable to those obtained by Watson, who determined the steady-state solution for radial and two-dimensional flows using a similarity solution [14]. In the work of Watson, $C = \pi/\sqrt{3} = 1.81$, which is smaller than the current value based on the leading-order mode. In contrast, the depth-averaging method gives $C = 2.5$, corresponding to the leading-order formulation in ε [2, 8]. It may thus be deduced that the current formulation (at least the steady-state solution) predicts a free-surface profile between that based on Watson's similarity solution and the depth-averaging profile. The current formulation thus gives an accuracy on the order of 8%, while conventional formulation based on the depth-averaging process gives a 30% error. The addition of higher-order modes leads even to a better accuracy. In fact, the inclusion of the second (cubic) mode alone leads to $C = 1.812$, which is in excellent agreement with Watson's similarity solution. The inclusion of the third- and higher-order modes leads sensibly to the same result (see also below). The close agreement with the similarity solution is a reflection of the robustness and reliability of the present approach, which is based on the Galerkin projection method. In fact, the depth-averaging formulation may be regarded as a special case of the present procedure, where only one mode is retained, but more importantly, a weight function equal to one is used instead of the quadratic polynomial, ϕ_1.

3. DISCUSSION AND RESULTS

The formulation and numerical implementation above are now applied to examine the early transients as the fluid emerges from the annulus, as schematically illustrated in Figure 1. The influence of inertia will be examined first. The influence of aspect ratio, substrate topography, as well as gravity, will then be investigated in some detail. In all calculations below, the domain of the fluid is assumed to extend from $x = 0$ to $x \to \infty$, but the domain of computation will be restricted to $x \in [0, 10]$, unless otherwise specified. Appropriate initial conditions are needed for the solution, namely, $\eta_0(x)$ and $U_0(x)$. Typically, in practice, at $t < 0$, there may be no fluid covering the substrate; all the fluid is still inside the annulus. At $t = 0$, the fluid begins to flow, with a (mean) velocity that is highest at $x = 0$. Theoretically, initial non-zero distributions in the surface height, $\eta(t = 0, x)$, and mean velocity, $U(t = 0, x)$, are needed to start the solution of the initial-value problem. Step functions in x may be envisaged. However, such initial distributions are discontinuous with respect to x. In most results in this study, the

initial free surface and velocity profiles are taken, respectively, as

$$\eta_0(x) = \begin{cases} 1 - 0.8\sin(\pi x/20), & 0 \leqslant x \leqslant 10 \\ 0.2, & x > 10 \end{cases}$$
$$U_0(x) = \begin{cases} 1 - \sin(\pi x/20), & 0 \leqslant x \leqslant 10 \\ 0, & x > 10 \end{cases} \tag{20}$$

Other initial conditions will also be considered. A similar single-harmonic initial condition for the free-surface shape was also used by Kalliadasis and Chang [18]. Moriarty *et al.* examined the gravity-induced deformation of a fluid occupying initially a parabolic domain (drop) with a constant thin film as tail [29]. In this study, conditions (20) are assumed for a straight substrate, and for a substrate of variable topography. These conditions correspond to an infinite fluid layer with a thickness that decays from one at $x = 0$, reaching 0.2 at $x = 10$ and remaining 0.2 for $x > 10$. The velocity is taken to diminish from one at $x = 0$, but vanishes for $x > 10$. These conditions also satisfy Equations (15). As will be discussed below, the influence of the initial conditions on the ensuing flow can be significant. Finally, the main parameters controlling the accuracy of the solution are the time increment, Δt, and the number of modes, M. These parameters were varied to cover the range $\Delta t \in [0.0125,\ 0.1]$ and $M \in [1, 4]$. In general, convergence is reached for $\Delta t < 0.025$ and $M < 3$. Another criterion for accuracy that is used is conservation of mass (volume) between the amount of fluid emerging from the annulus and that deployed on the rigid substrate. Calculations show that the error in mass is generally to within 1%. The tolerance on the Runge–Kutta scheme is set as 10^{-5}.

3.1. *Influence of inertia*

Consider now the general flow response for a fluid at moderately high Reynolds number. It is important to simultaneously assess first the convergence and accuracy of the numerical solution. For this, consider the flow at $Re = 100$, when non-linear effects are significant. The annulus aspect ratio is fixed at $\varepsilon = 0.1$, and gravity is assumed to be negligible ($Fr \to \infty$). In this section, the substrate is straight ($h = 0$). The flow behaviour is examined over a period of 4 time units. It is generally found that interesting dynamics arise for $t < 4$, without pronounced curvature effects manifesting themselves at the free surface. The behaviour in Figure 2 typically illustrates the response in the early stages for a flow with high-inertia. The evolution of the free surface is shown in Figure 2(a) for the projection of the flow in the (x, z) plane. The figure shows the free surface at equal intervals of 0.4 time units, including the initial profile ($t = 0$). The steady-state profile is also shown in the figure (dashed curve), which exhibits a linear growth with x (in accord with Equation (19) for two-dimensional flow). A three-dimensional perspective is shown in Figure 3, at two stages $t = 1$ and 4. Figure 2 shows that there is a strong radial flow that leads to the formation of a solitary wave, similarly to that encountered under steady-state conditions for gravity-driven flow [37]. Figure 2(a) shows that after $t = 4$, the trailing edge of the wave ($x < 3$) has already attained the steady-state shape. There is an accumulation of fluid in the radial direction, the origin of which becomes clearer as the velocity coefficients are examined. As will be seen below, this build-up of fluid is typical and is strongly influenced by inertia. The stagnation of the film height at $x = 10$ originates from

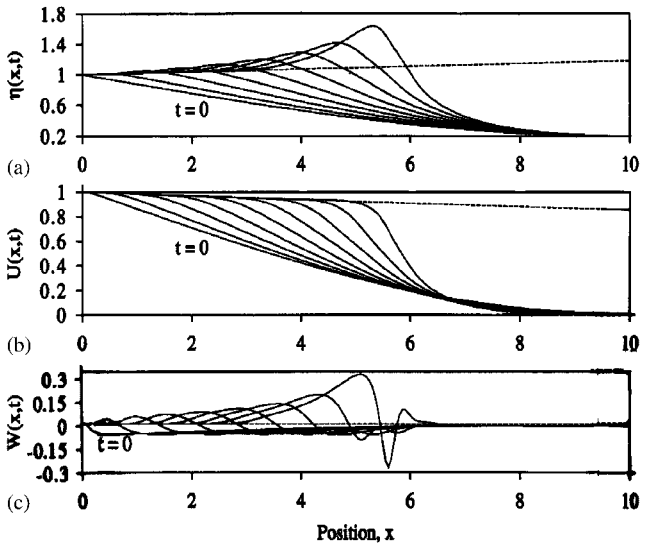

Figure 2. Transient flow response with high inertia in the absence of gravity ($Fr \to \infty$), for $Re = 100$ ($\varepsilon = 0.1$), over a straight cylindrical substrate. The figure shows (a) the evolution of the free surface, (b) mean axial and (c) radial velocity components, at equal intervals over a period of 4 time units, including the initial conditions ($t = 0$). Also shown is the steady-state profile (dashed line).

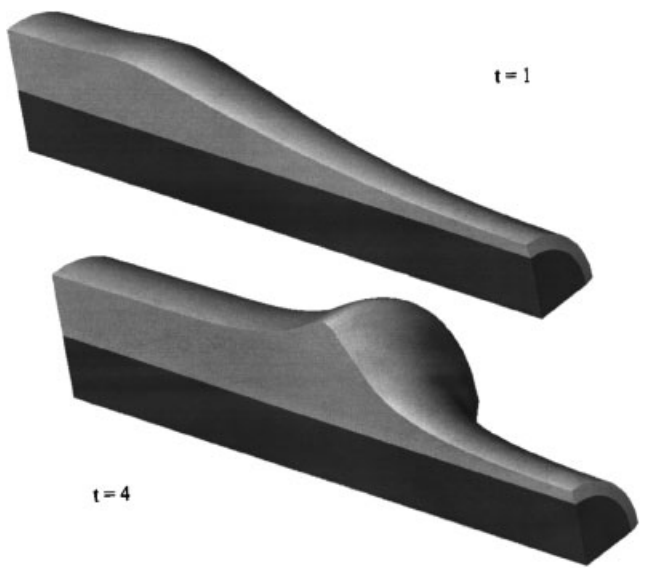

Figure 3. Three-dimensional perspective of high-inertia film flow, $Re = 100$ and $\varepsilon = 0.1$, for a flow over a straight cylindrical substrate, at two stages, $t = 1$ and 4 ($Fr \to \infty$).

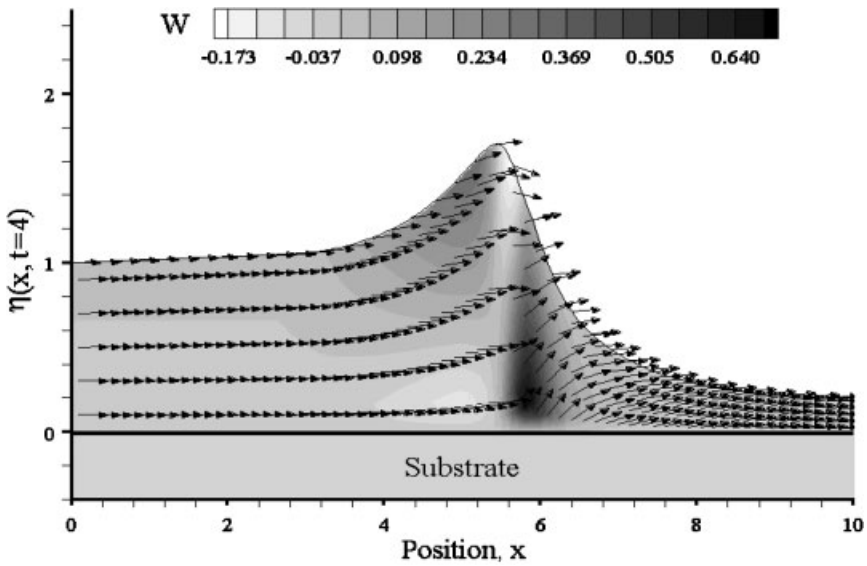

Figure 4. Flow field and contours of the radial velocity component, $w(x,z,\ t=4)$ for high-inertia flow, $Re=100$ ($\varepsilon=0.1$), for a straight cylindrical substrate ($Fr\to\infty$).

the initial conditions (20) used (see below). The corresponding profiles for the mean velocity components in the axial and radial directions, $U(x,t)$ and $W(x,t)$, are shown, respectively, in Figures 2(b) and 2(c). The steady-state velocity distributions are also shown, which are again linear over the range of fluid shown (dashed curves). In the early stages, U decreases almost linearly as the fluid emerges from the annulus, to then asymptotically vanish as the fluid approaches the straight end of the free surface at $x=10$. With time, however, the flow exhibits a sharp drop as the wave steepens. This drop is a reflection of strong elongational flow or normal stress as in converging/diverging flow. There is simultaneously a strong radial normal stress as Figure 2(c) indicates. The radial flow increases overall in strength as the fluid moves downstream, and, unlike the axial flow, reaches a maximum at the crest of the surface wave. As the free surface deforms further, W exhibits a maximum at the tail of the wave, a minimum at the crest, a relatively weak maximum ahead of the crest, to then asymptotically vanish downstream. There is a considerable gain in strength in radial flow with time, reaching one third of the axial flow. However, the steady radial flow is weak and essentially constant over the fluid domain. The significance of the radial flow is further appreciated from Figure 4, which depicts the flow field and the contours of the radial velocity component, $w(x,z,t=4)$, at an advanced stage. The flow field indicates clearly the sudden change in direction that flow takes below the crest ($5.5<x<6$), where a strong radial flow develops near the substrate, along with a strong inward flow below the wave crest. It is clear from Figures 2(c) and 4 that the radial flow is not negligible as the long-wave approximation suggests [38].

There are two remarkable features in the evolution of the film profile shown in Figure 2(a). One is the continuous build-up and propagation of the wave front, and second the steady-state swept by the tail of the wave front. The question then arises as to whether the steady-state profile is ever reached over the long time. The current thin-film results, subject to the chosen

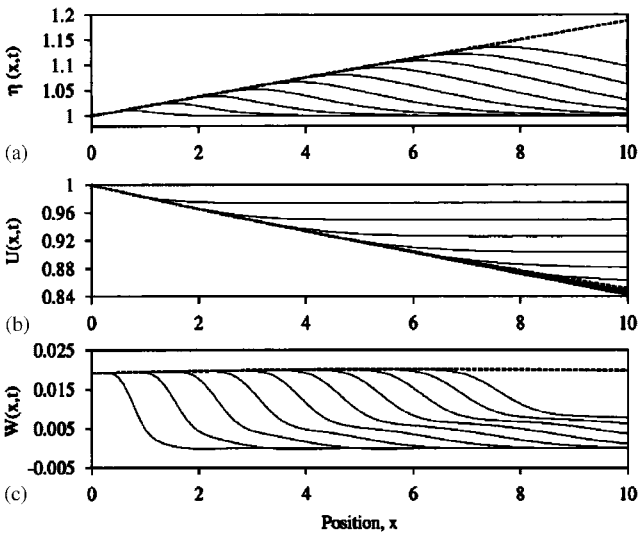

Figure 5. Transient flow response with high inertia in the absence of gravity ($Fr \to \infty$), for $Re = 100$ ($\varepsilon = 0.1$), over a straight cylindrical substrate. Uniform initial conditions are used. The figure shows (a) the evolution of the free surface, (b) mean axial and (c) radial velocity components, at equal intervals over a period of 10 time units, including the initial conditions ($t = 0$). Also shown is the steady-state profile (dashed line).

initial and boundary conditions, and in the absence of surface tension, clearly indicate that the steady profile will simply never be reached. In reality, some additional mechanism is needed to halt the wave growth, such as surface tension and/or gravity effects [18]. Pronounced growth will also result in the breakdown of the thin-film assumption.

The fluid build-up illustrated in Figure 2 can be completely annihilated for some other initial conditions. Uniform initial surface height and Poiseuille profile for the streamwise velocity are such conditions. In this case, $\eta(x, t = 0) = 1$ and $U(x, t = 0) = 8/(8 + 5\varepsilon)$. Figure 5 shows the response for $Re = 100$ and $\varepsilon = 0.1$. The profiles are shown for a duration of 10 time units, at equal intervals. There are two striking differences in comparison to Figure 2. The first difference is the lack of fluid build-up or elevation of the free surface, despite the formation and propagation of a surface wave. The surface rises with time in Figure 5(a), with the wave tail tracing the steady state, but the transient surface height is always below the steady level. The second important difference with the situation in Figure 2(a) is the stability of the steady state. The initial disturbance is evolving monotonically toward the steady free-surface profile. The streamwise velocity (Figure 5(b)) as well as the depthwise velocity decreases monotonically with position, reaching a constant level. It is interesting to note that in this case, W does not exhibit a maximum as in Figure 2(c). It is important to observe that the profiles in Figure 6 indicate that the steady state is stable to the initial perturbation. Inertia is found to have a significant influence on the flow, the shape of the free surface, the wave formation and speed of propagation. In case of low-inertia flow, a considerable steepening of the wave occurs, with a significant accumulation of the fluid near the annulus exit. Unlike high-inertia flow (Figure 2), the wave tends to remain relatively stationary. The steady-state

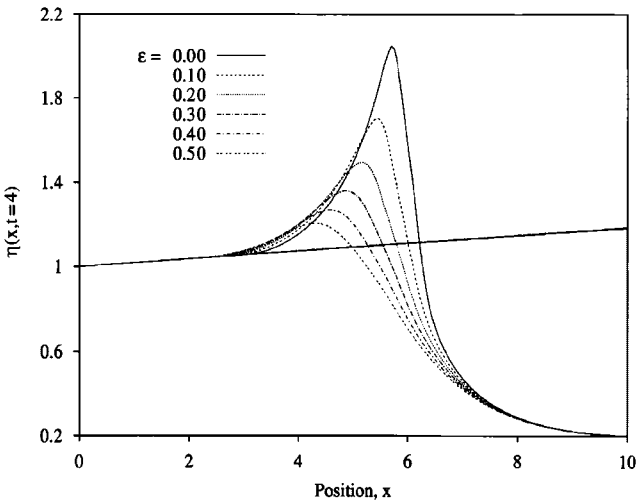

Figure 6. Influence of annulus aspect ratio, for the range $\varepsilon \in [0, 0.5]$, on the shape of the free surface at $t = 4$, for high-inertia flow ($Re = 100$). The steady states are included ($Fr \to \infty$). The cylindrical substrate is assumed to be straight.

profile indicates clearly the difficulty of the fluid to move forward. This is of course expected for a highly viscous fluid. The flow is halted near the annulus exit, with the streamwise velocity dropping sharply not far from $x = 0$ (see Reference [41] for two-dimensional coating case). The rise in free-surface level is directly due to normal stress effect. The flow behaves similarly to that through a sudden expansion; shear effects are dominated by elongational effects. This is particularly evident from solution (19), which shows that the steady-state streamwise flow is essentially annihilated for creeping flow ($Re \to 0$), resulting in 90° expansion of the film ($\eta_S \to \infty$) near the annulus. Calculations show that the film generally grows like $1/Re$ (for two-dimensional flow) for both steady and unsteady states. Expressions (19) indicate that elongational effect behaves like $1/x^2$ for small Re. As a result, there is a considerable increase in radial flow as well. The extreme exhibited by W in Figure 2(c) are accentuated and become more localized as viscous effects become dominant. The radial velocity component cannot be neglected as is done in some of the work in the literature [48], especially for low-inertia flow. Figure 5 indicates a higher degree of symmetry that is reached near the crest of the wave at low Re (compare with Figure 2(a)). At low Re, the symmetry-breaking convective term UU_X is dominated by the symmetric diffusive terms.

3.2. *Influence of annulus aspect ratio*

The influence of the aspect ratio is illustrated for a moderately high-inertia flow ($Re = 100$) for a straight cylindrical substrate. Gravity is still assumed to be negligible. The response of the free-surface shape at $t = 4$ is shown in Figure 6 for the range $\varepsilon \in [0, 0.5]$. It is important to remark that this range of values for the aspect ratio exceeds the range of validity of the thin-film approximation, where terms of $O(\varepsilon^2)$ are assumed to be negligible. Moreover, and as discussed earlier, thick films are likely to become unstable. However, this wide range is

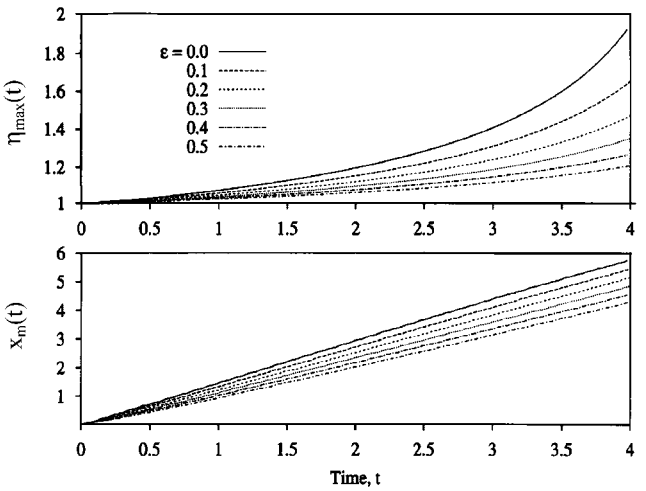

Figure 7. Influence of annulus aspect ratio, for the range $\varepsilon \in [0, 0.5]$, on the evolution of the crest height, $\eta_{\max}(t)$, and corresponding position, $x_m(t)$, for high-inertia flow ($Re = 100$, $Fr \to \infty$). The cylindrical substrate is assumed to be straight.

used here and in subsequent figures only for clarity of presentation. The results shown may even be *quantitatively* inaccurate, and are important as they point to the qualitative trend expected when more realistic values of ε are used. The influence of the terms neglected in the momentum conservation equations, leading to Equation (4), is assessed for simple gravity-driven one-dimensional flow. In this case, the exact solution reads

$$u(z) = -\frac{Re}{2\varepsilon Fr^2}\left[\frac{\varepsilon}{2}z^2 + z - \frac{(\varepsilon+1)^2}{\varepsilon}\ln(\varepsilon z + 1)\right] \tag{21}$$

which should be contrasted with the solution of Equation (4), namely

$$u(z) = -\frac{Re}{\varepsilon Fr^2}\left[z + \frac{e^{\varepsilon}}{\varepsilon}(e^{-\varepsilon z} - 1)\right] \tag{22}$$

It is found that the maximum error generated from using (22) is 0.2% for $\varepsilon = 0.1$ and 3.5% for $\varepsilon = 0.5$, which indicates that the results in Figure 6 may be quantitatively reasonable. The steady-state profiles in the figure appear to be uninfluenced by aspect ratio. Moreover, the mean axial flow is not expected to be significantly affected by ε, according to Equation (17). It is clear from the figure that the substrate curvature tends to prohibit wave formation. To a lesser extent, the wave propagation is also delayed for the higher aspect ratio. The crest height decreases relatively sharply as ε increases from zero (that is, from the two-dimensional limit). The coating of a wire-like substrate is thus easier to achieve than that of a thick cylinder. This is also confirmed by inspecting the flow in the axial and radial directions (not shown). Unlike the axial flow, the radial flow experiences a drastic drop as ε increases.

The influence of annulus aspect ratio is also significant on the crest height and wave speed. Figure 7 displays the evolution of $\eta_{\max}(t)$ and corresponding position, $x_m(t)$, with time. For two-dimensional flow, x_m is linear with t, and the wave advances at a constant speed, which

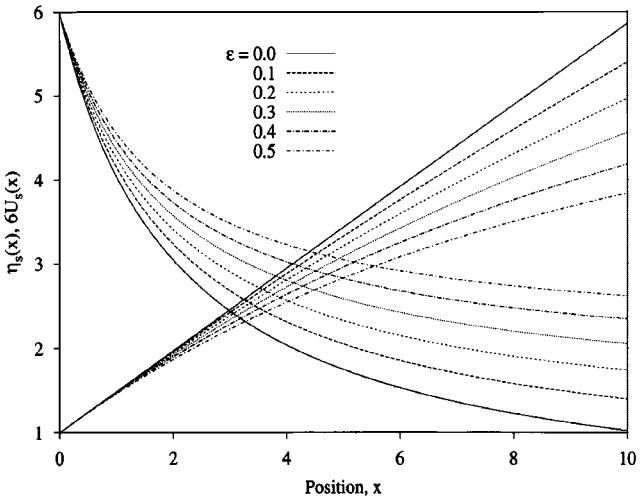

Figure 8. Influence of annulus aspect ratio, for the range $\varepsilon \in [0, 0.5]$, on the steady free-surface profile and corresponding mean velocity, for low-inertia flow ($Re = 4$, $Fr \to \infty$).

is equal to 1.36 in this case. The crest height increases at a rate that accelerates with time. As ε increases from zero, the wave speed tends to be smaller upon inception, but eventually approaches the same constant level (1.36), corresponding to two-dimensional flow, for large t.

It is interesting to observe in conclusion that although the fluid exhibits a significant drop in surface height for a cylinder of smaller diameter, the wave speed is the same (asymptotically) regardless of the annulus aspect ratio. It is finally observed from Figure 7 that, at a given time t, the crest height increases exponentially with ε, while its position increases linearly with ε. The rate of front advancement depicted in the figure may be compared to the rate of radial spreading examined by Wilson *et al.*, who studied the effect of slip coefficient. Obviously, any comparison (though remote) with the current results should be made with the case $\varepsilon = 0$ [13]. The results of Wilson *et al.* suggest that for the smallest slip coefficient considered, the rate of spreading approaches a linear spread similarly to the curve $\varepsilon = 0$ in Figure 8. The absence of influence of the annulus aspect ratio on the steady-state film profile is somewhat perplexing, and yet the strong influence of ε on the unsteady profiles is clearly present as indicated by Figure 6. The effect of ε on the rate of change of η can be, to some extent, assessed from Equation (13), which predicts the rate of growth of the film should get smaller as the annulus ratio is increased; this is clearly the case in Figures 6 and 7. In contrast, for steady-state flow the relation between U and η does not depend on ε, as Equation (17) suggests. If, further, inertia is dominant, the only term where ε occurs is due to curvature effect in the continuity equation (3), which is not expected to be significant since the radial velocity component is relatively weak throughout the film. If, however, inertia is not dominant, then the influence of the annulus ratio will be reflected more significantly through the curvature diffusive term, εu_z, in Equation (4). This term is a reflection of the shear stress, which is generally significant, especially near the substrate. Figure 8 displays the significant influence of the annulus ratio on the steady-state surface profiles and corresponding velocity distributions for $Re = 4$. In

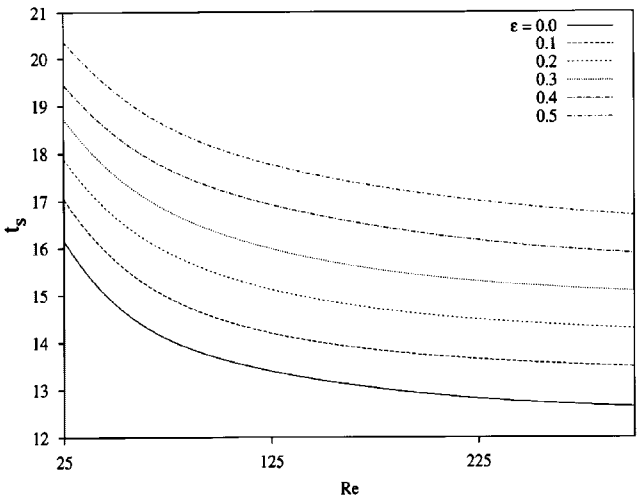

Figure 9. Influence of annulus aspect ratio, for the range $\varepsilon \in [0, 0.5]$, on the time, t_S, an initially uniform film takes to reach steady-state conditions ($Fr \to \infty$).

particular, the η_S profiles show that the film thickness decreases from the two-dimensional linear growth as ε increases. The film thickness as well as the mean axial velocity tends to level off downstream for large ε. The figure thus indicates that wires with relatively smaller diameter are easier to coat.

Finally, it was observed from Figure 5 that the steady state is stable to a perturbation corresponding to uniform initial conditions. This means that the steady state is eventually reached after some time, which depends on the various geometrical and flow parameters. Figure 9 shows the influence of the aspect ratio on the time, t_S, the flow takes to reach steady state. Steady state is assumed to be reached when the evolving free surface is within 0.01%. The figure shows the behaviour of t_S as function of Re for $\varepsilon \in [0, 0.5]$, and it is found that t_S decreases monotonically with Re, slowly for small Re and eventually leveling off. Thus, for a moderately high-inertia fluid, t_S becomes independent of the Reynolds number. The figure also indicates that t_S increases with ε, almost linearly at large Re. The curves may appear to be similar, but in fact are not.

3.3. *Influence of substrate topography*

The influence of substrate topography is examined for step changes in the bottom profile. The steps, however, must be smooth given the thin-film hypothesis, which asserts, in addition to the small film thickness, that the substrate and film geometry must be continuous. A suitable substrate profile is taken from Reference [30], which is rewritten here in dimensionless form as

$$h(x) = A\left[\frac{1}{2} + \frac{1}{\pi}\tan^{-1}\left(\frac{x - x_0}{\delta}\right)\right] \tag{23}$$

where A is the amplitude of the step, δ is the slope, x_0 is the location of the step. In this work, $x_0 = 4$ and $\delta = 0.5$. It is found that both the step-up and step-down disturbances have a

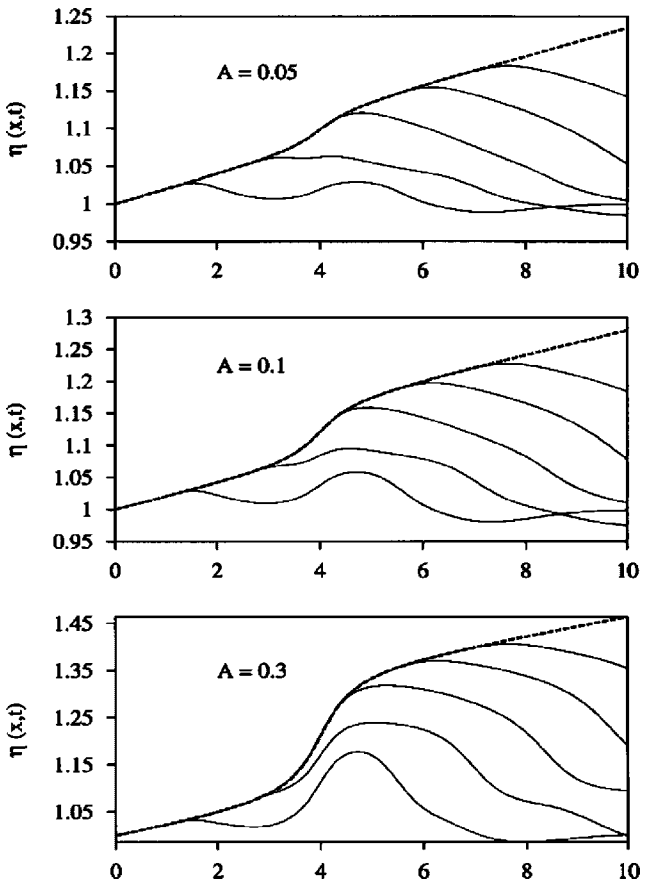

Figure 10. Influence of step amplitude on the transient flow response with high inertia in the absence of gravity ($Fr \to \infty$), for $Re = 100$ ($\varepsilon = 0.1$), over a substrate with step-up. The figure shows the evolution of the free surface at equal intervals over a period of 10 time units for different amplitudes, including the steady-state profile (dashed line).

significant and different influence on the flow. In this section, uniform initial conditions will be assumed. Thus, the initial free surface is given by $\eta(x, t = 0) = 1$.

Consider first the influence of the step-up profile. The evolution of the free surface for a high-inertia flow is shown for three step amplitudes in Figure 10, corresponding to $A = 0.05$, 0.1 and 0.3. The Reynolds number is fixed to $Re = 100$ and $Fr \to \infty$. The steady-state profiles are included (dashed curve). The substrate topography is not shown. The profiles in Figure 10 are plotted at equal intervals over 10 time units, and should be compared to those in Figure 5 for a straight cylindrical substrate. The presence of the step causes the surface wave to exhibit a secondary wave that is detached from the steady profile, and moves downstream from the primary wave. The tail and crest of the primary wave follow closely the steady profile. As the step increases, the secondary wave steepens, leading to the formation of a square wave. More importantly, the steady state appears to remain stable with respect to the initial (uniform) disturbance despite the presence of a perturbation in the substrate.

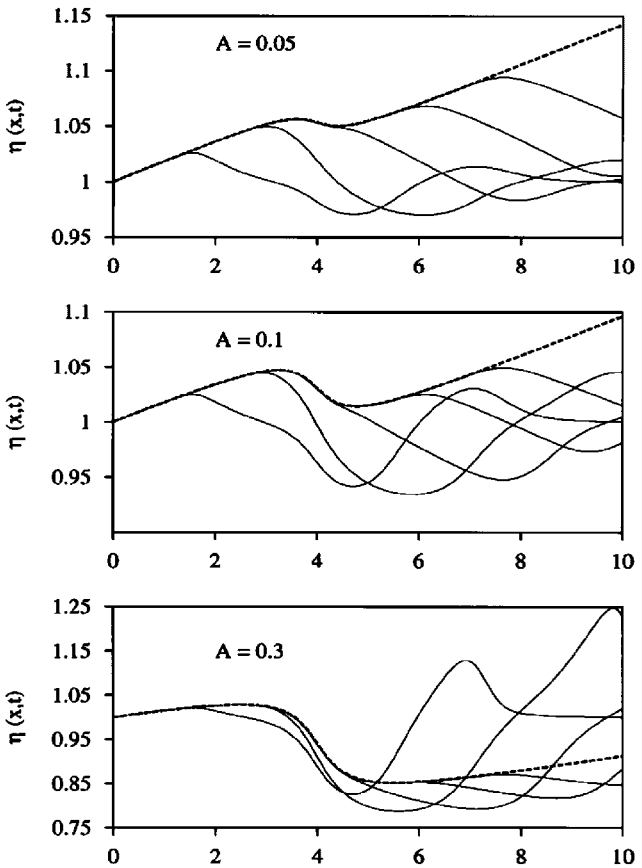

Figure 11. Influence of step amplitude on the transient flow response with high inertia in the absence of gravity ($Fr \to \infty$), for $Re = 100$ ($\varepsilon = 0.1$), over a substrate with step-down. The figure shows the evolution of the free surface at equal intervals over a period of 10 time units for different amplitudes, including the steady-state profile (dashed line).

The stability of the steady state is not unconditional to the type of perturbation in the substrate. This is clearly illustrated in the case of a step-down in the substrate. The resulting flow behaviour is shown in Figure 11, where the profiles are depicted for the same parameters as in Figure 10. In this case, the secondary wave travelling downstream grows significantly with step amplitude, and eventually exceeds the steady-state level, reflecting fluid build-up with time, similarly to the flow in Figure 2. Clearly in this case, the steady-state flow is unstable although the same (uniform) initial conditions are used as for the step-up geometry.

The steady-state profiles in Figures 10 and 11 reflect closely the shape of the substrate, showing a free-surface elevation entirely commensurate with that of the step. This response is reminiscent of the two-dimensional results reported by Kalliadasis *et al.* [30], who neglected inertia but included surface tension effects, which led to the formation of ridges and depressions in the vicinity of the step. These, however, are usually localized with little overall influence on the film profile. Moreover, surface tension does not seem to strongly deviate

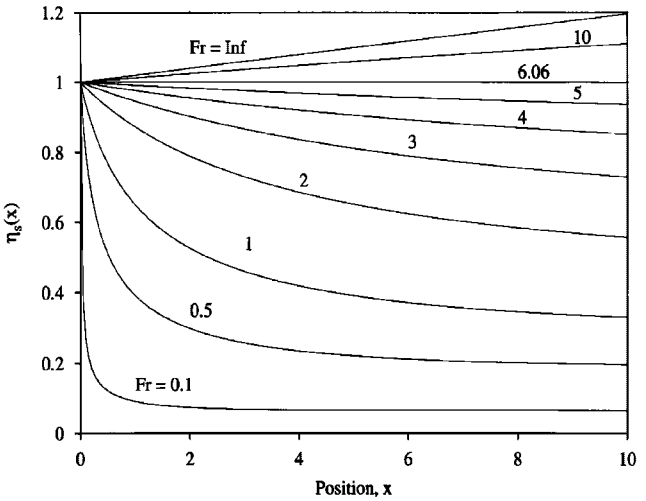

Figure 12. Influence of gravity on the steady-state profiles of the free surface, for $Re = 100$ and $\varepsilon = 0.1$. The curves are shown for the range $Fr \in [0.1, \infty]$.

the shape of the film surface from that of the disturbance. Figures 10 and 11 of Kalliadasis *et al.* show that this is the case for both mounds and trenches [30]. Figure 12 illustrates the influence of inertia on the steady-state shape of the free surface for both a step-up and a step-down in the substrate.

3.4. Influence of gravity

Unlike two-dimensional flow problems commonly found in the literature, in this case, gravity acts in the direction of axial flow. In fact, this makes the gravity term easier to handle as it is decoupled from the surface height. However, the effect of gravity can be significant even though it is present as a constant source term in Equation (14). Some insight may be preliminarily gained by examining the two-dimensional steady-state flow. In this case, the equation for the free-surface profile becomes

$$\frac{\mathrm{d}\eta_s}{\mathrm{d}x} = \frac{C}{Re}\left(1 - \frac{Re}{3Fr^2}\,\eta_s^3\right) \tag{24}$$

The presence of gravity will thus, in general, force the free surface to deviate from the linear form given by Equation (19). At a critical Froude number, $Fr_c = \sqrt{Re/3}$, the slope at the annulus exit is zero, and remains zero for $x > 0$. In this case, viscous and gravity forces are in balance. For $Fr > Fr_c (Fr < Fr_c)$, the surface slope at the exit is positive (negative), and decreases (increases) with x until it vanishes at a certain position, $x = x^*$, and the film thickness remains constant further downstream ($x > x^*$). The position x^* corresponds to a free surface level $\eta_s^* \equiv \eta_s(x^*) = \sqrt[3]{3Fr^2/Re}$.

The situation turned out, expectedly, to be similar for axisymmetric flow, especially when the aspect ratio, ε, is very small. The influence of gravity is thus assessed numerically by varying the Froude number and keeping the other parameters fixed. Figure 13 illustrates typically

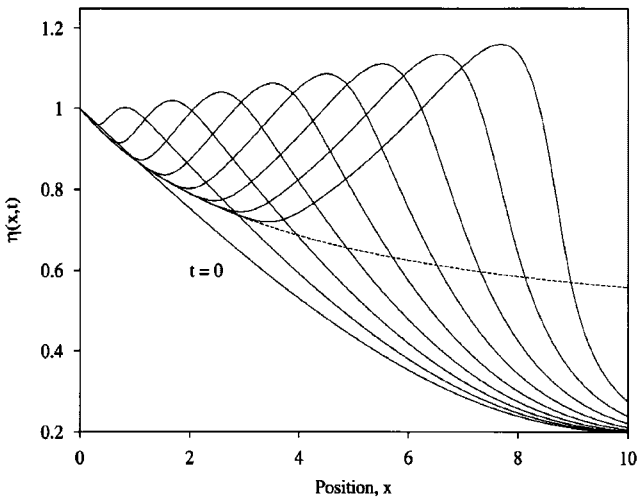

Figure 13. Evolution of the free surface with time for high-inertia flow, $Re = 100$ ($\varepsilon = 0.1$), for a flat substrate, in the presence of strong gravity effect ($Fr = 2$). The figure shows the free surfaces at equal intervals over a period of 4 time units, including the initial surface. The steady-state profile (dashed line) is also shown.

the influence of gravity on the steady-state free-surface profiles for the range $Fr \in [0.1, \infty]$, with the Reynolds number fixed at $Re = 100$, and the aspect ratio at $\varepsilon = 0.1$. Here $h = 0$. It is recalled that in the absence of gravity ($Fr \to \infty$), $\eta_s(x)$ grows linearly with x (at least for two-dimensional flow). The critical Froude number is very close to $Fr_c = 6$, which is slightly higher than that corresponding to two-dimensional flow ($Fr_c = 5.77$). When gravity effect is dominant, η_s decreases similarly to the prediction of Equation (24). In this case, the critical surface level is estimated from two-dimensional flow to be approximately $\eta_s^* = \sqrt[3]{0.03\,Fr^2}$. The surface level for $Fr = 0.1$ is expected to reach constant level when η_s reaches approximately 0.067, which is very close to the constant level reached by the curve $Fr = 0.1$ in Figure 12.

The influence of gravity is even more significant under transient conditions. The flow response is typically illustrated in Figure 13 for $Re = 100$, $\varepsilon = 0.1$ and $Fr = 2$. In contrast to the flow in the absence of gravity (Figure 2(a)), the free surface begins to immediately collapse towards the steady-state level upon the fluid exiting the annulus. However, the maximum in free surface remains significantly higher above the steady-state level than when gravity is absent. Interestingly, $\eta_{\max}(t)$ does not grow as fast as in Figure 2(a). In fact, Figure 14 shows that the growth in the surface crest height is linear with time. The situation is similar to that reported by Moriarty *et al.* for a fluid drop deforming under gravity [29]. The draining drop tends to deform significantly, while the drop tip remains essentially at the same height (see Figures 2 and 12 in Reference [29]). For a flow with weaker inertia, the arguments for two-dimensional flow suggest that the film reaches a constant level earlier. Figure 14 displays the film evolution for $Re = 4$, $Fr = 2$ and $\varepsilon = 0.1$. It is clear, upon comparison with Figure 5, that gravity, like inertia, makes the coating process achievable. Gravity tends to be most influential far downstream from the annulus exit.

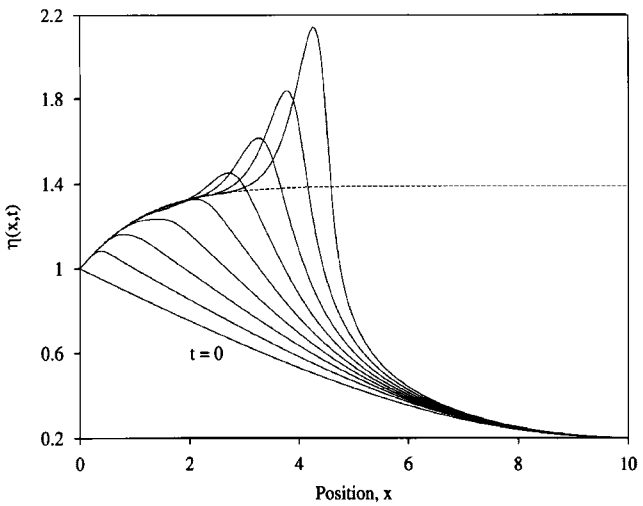

Figure 14. Evolution of the free surface with time for low-inertia flow, $Re = 4$ ($\varepsilon = 0.1$), for a flat substrate, in the presence of strong gravity effect ($Fr = 2$). The figure shows the free surfaces at equal intervals over a period of 4 time units, including the initial surface. The steady-state profile (dashed line) is also shown.

The influence of gravity is also significant for a substrate of variable shape. Here again the cases of a step-up and a step-down will be considered for a flow with uniform initial conditions. Figures 15 and 16 shows the influence of gravity for both geometries for the range $Fr \in [1, \infty]$. The influence of gravity is found to be significant for both transient and steady flows. For a step-up (Figure 15), the steady profiles deviate gradually from the substrate geometry as gravity effect increases. In particular, the steady profile exhibits a pronounced thinning of the film near the annulus exit with gravity. Simultaneously, the transient profiles shift from below to above the steady state. For a step-down (Figure 16), the steady film thickness decreases with gravity, with the surface becoming smoother. The figure indicates that the secondary wave decreases in amplitude, reflecting a stabilization of the steady state.

4. CONCLUSION

Pressure-driven axisymmetric flow of a thin fluid film, emerging from an annulus, is examined in this study. Early transient behaviour is emphasized. The initial conditions, annulus aspect ratio, substrate topography, gravity, as well as inertia effects are investigated in some detail. Although the focus of the study is mainly on transient behaviour, the steady-state flow is also examined for reference. The flow is governed by the thin-film equations of the 'boundary-layer' type, which are solved by expanding the flow field in orthonormal modes over the depth. The Galerkin projection method is applied to generate the equations that govern the expansion coefficients. The method generalizes and improves the approach proposed earlier by Zienkiewicz and Heinrich [48]. It is found that reasonable convergence is generally achieved when less than three or four modes are included. The formulation reduces to the

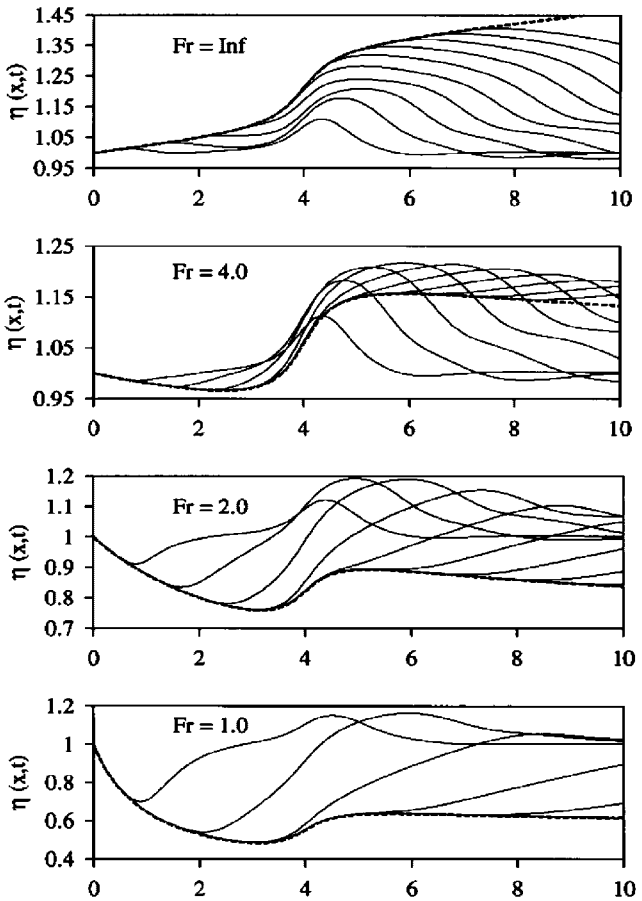

Figure 15. Influence of gravity on the transient flow response with high inertia for $Re = 100$ ($\varepsilon = 0.1$), over a substrate with step-up. The figure shows the evolution of the free surface at equal intervals over a period of 10 time units, including the steady-state profile (dashed line), for $Fr \in [1, \infty)$.

depth-averaging procedure in two-dimensions when only the leading-order mode, with a weight function equal to one, is used. It is shown that, in the limit of two-dimensional steady flow, there is excellent agreement with the similarity solution of Watson [14]. Only two modes are required to reach an agreement to the third decimal. The improvement of the proposed approach over the conventional depth-averaging technique is mainly owing to the use of appropriate weighting functions (to minimize the residual error), and, to a lesser, to the choice of orthonormal modes. In this work, Chandrasekhar functions are used, but other shape functions, such as simple polynomials or trigonometric modes, appear to lead essentially to the same level of accuracy [41].

Initial conditions are found to have a significant effect on the flow. Non-uniform conditions on the streamwise velocity and film surface lead unavoidably to fluid build-up upon exiting the annulus, leading to the formation of a solitary wave that propagates downstream at a

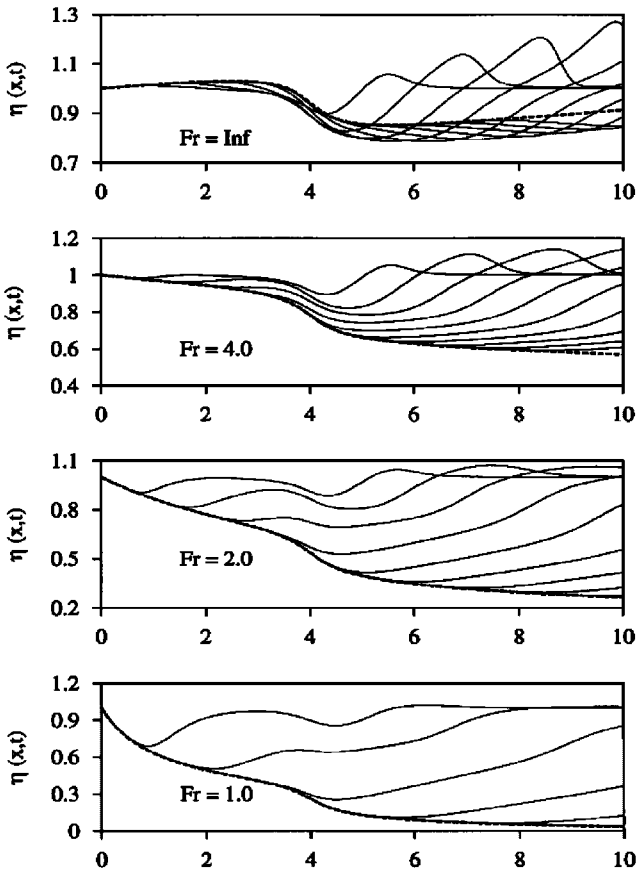

Figure 16. Influence of gravity on the transient flow response with high inertia for $Re = 100$ ($\varepsilon = 0.1$), over a substrate with step-down. The figure shows the evolution of the free surface at equal intervals over a period of 10 time units, including the steady-state profile (dashed line), for $Fr \in [1, \infty)$.

rate that depends strongly on inertia. Typically, the flow exhibits a significant drop in axial velocity, accompanied by a surge in radial velocity, at the wave front. Elongational flow is clearly important in this case, in addition to the significant shearing that is expected in thin-film flow. While a high-inertia fluid propagates downstream, exhibiting a wave of crest height on the order of the substrate depth (Figure 2), a low-inertia fluid tends to stagnate near the annulus exit, exhibiting a standing wave with a crest height that grows with time, and a base width on the order of cylindrical substrate radius. The radial flow is found to be significant for all flow configurations considered, particularly under transient conditions. Hence, for strongly transient flow, Benney's long-wave approximation becomes inadequate, even when *Re* is small [42]. This clearly contrasts what may be suggested in the literature [38]. Note, however, that for steady state, radial flow is found to be insignificant for a straight cylindrical substrate. This is of course expected as elongational effects are negligible, at least when gravity is negligible.

The influence of initial conditions on the subsequent motion is found to be important. In this work, the fluid domain is assumed to correspond to an initial fluid layer, with thickness decreasing downstream until it reaches a constant level. The initial velocity is assumed to be strongest at the annulus exit, to decay downstream and vanish when the film reaches constant thickness. In this case, an asymmetric wave forms, which steepens as it travels downstream. While the tail of the wave reaches steady state, the wave front continues to steepen with wave growth. Under these conditions, steady-state conditions are clearly never reached. However, the film assumption is bound to break down with further growth, and surface tension effects, which may be negligible initially, become eventually important. Other initial conditions are also examined, showing similar behaviour. In contrast, the transient response is found to be stable for uniform initial conditions in mean velocity and film profile (Figure 5). In this case, there is no fluid build-up, and the wave is always located beneath the steady state. For a variable substrate, the steady state may not be stable to uniform initial conditions (see below).

The effect of geometry is examined by varying the annulus aspect ratio, ε, and substrate topography. It is found that, for steady state, high-inertia flow responds very closely to two-dimensional flow (see also Reference [14]). This is particularly true for the shape of the film. Thus, the final coating thickness of large- and small-diameter wires is similar when inertia is significant. However, for small inertia, the (steady) film thickness decreases linearly with ε, reaching a constant (asymptotic) level far downstream (Figure 5). Transient behaviour is significantly reduced with ε, for high- and low-inertia flows (Figures 6–8). Two types of perturbations, a step-up, and a step-down, are used to study the influence of substrate topography. The results are contrasted with those of Kalliadasis *et al.* for steady flow [30]. Inertia, step amplitude, and initial conditions are found to have a significant influence on the response of the flow in the presence of the perturbations. It is observed that the flow of a high-inertia fluid over a step-down exhibits the formation of a secondary wave that moves upstream of the primary wave (Figure 11). While the steady state appears to be always stable to uniform initial film for a step-up (Figure 10), it becomes unstable for high-amplitude step-down (Figure 11).

Finally, the influence of gravity is examined for straight and variable substrates. The steady-state film thickness changes from a linear growth with axial position when gravity is weak, to a sharp drop near the annulus exit at small Fr value. The situation is very similar to two-dimensional flow, which indicates that the thickness reaches a constant level equal to $\sqrt[3]{3\,Fr^2/Re}$ far downstream from the annulus exit. It is also found that, at a critical Froude number, $Fr_c = \sqrt{Re/3}$, the film thickness remains the same at any position (see Figure 12). In this case, viscous and gravity effects are in complete balance. Gravity tends, as expected to precipitate the flow, attenuating wave formation. In this case, the wave grows linearly with position and time, as opposed to the much faster growth rate experienced in the absence of gravity (compare Figures 2 and 13). Gravity is found to have a stabilizing influence for a step-down substrate (Figure 16).

ACKNOWLEDGEMENTS

This work was supported by the Natural Sciences and Engineering Research Council of Canada.

REFERENCES

1. Voit SS, Tsunamis. *Annual Review of Fluid Mechanics* 1987; **19**:217.
2. Chang HC. Wave evolution on a falling film. *Annual Review of Fluid Mechanics* 1994; **26**:103.
3. Oron A, Davis SH, Bankoff SG. Long-scale evolution of thin liquid film. *Reviews of Modern Physics* 1997; **69**:931.
4. Kistler SF, Schweizer PM. *Liquid Film Coating*. Chapman & Hall: London, UK, 1997.
5. Meyers TG. Thin films with high surface tension. *SIAM Review* 1998; **40**:441.
6. Quéré D. Thin films flowing on vertical fibers. *Europhysics Letters* 1990; **13**:721.
7. Alekseenko SV, Nakoryakov VE, Pokusaev BG. Wave formation on a vertical falling liquid film. *A.I.Ch.E Journal* 1985; **31**:1446.
8. Prokopiou T, Cheng M, Chang HC. Long waves on inclined films at high Reynolds number. *Journal of Fluid Mechanics* 1991; **222**:665.
9. Frenkel AL. Nonlinear theory of strongly undulating thin films flowing down vertical surfaces. *Europhysics Letters* 1992; **18**:583.
10. Davalos-Orozco LA, Davis SH, Bankoff SG. Nonlinear instability of a fluid layer flowing down a vertical wall under imposed time-periodic perturbations. *Physical Review E* 1997; **55**:374.
11. Ruyer-Quil C, Manneville P. Modeling film flows down inclined planes. *European Journal of Physics B* 1998; **6**:277.
12. Nguyen LT, Balakotaiah V. Modeling and experimental studies of wave evolution on free falling viscous films. *Physics of Fluids* 2000; **9**:2236.
13. Wilson SK, Hunt R, Duffy BR. The rate of spreading in spin coating. *Journal of Fluid Mechanics* 2000; **413**:65.
14. Watson EJ. The radial spread of a liquid jet over a horizontal plane. *Journal of Fluid Mechanics* 1964; **20**:481.
15. Spaid MA, Homsy GM. Viscoelastic free surface flows: spin coating and dynamic contact lines. *Journal of Non-Newtonian Fluid Mechanics* 1994; **55**:249.
16. McKinley IS, Wilson SK, Duffy BR. Spin coating and air-jet blowing of thin viscous drops. *Physics of Fluids* 1999; **11**:30.
17. Duffy BR, Wilson SK. Thin-film and curtain flows on the outside of a rotating horizontal cylinder. *Journal of Fluid Mechanics* 1999; **394**:29.
18. Kalliadasis S, Chang HC. Drop formation during coating of vertical fibers. *Journal of Fluid Mechanics* 1994; **261**:135.
19. Mashayek F, Ashgriz N. Instability of liquid coatings on cylindrical surfaces. *Physics of Fluids* 1995; **7**:2143.
20. de Bruyn JR. Crossover between surface tension and gravity-driven instabilities of a thin fluid layer on a horizontal cylinder. *Physics of Fluids* 1997; **9**:1599.
21. Szeri AZ. Some extensions of the lubrication theory of Osborne Reynolds. *Transactions of ASME Journal of Tribology* 1987; **109**:21.
22. Hayashi H. Recent studies on fluid film lubrication with non-Newtonian lubricants. *JSME International Journal Series III* 1991; **34**:1.
23. Larson RG. Instabilities in viscoelastic flows. *Rheology Acta* 1992; **31**:213.
24. Ross AB, Wilson SK, Duffy BR. Blade coating of a power-law fluid. *Physics of Fluids* 1999; **11**:958.
25. Khayat RE. Transient two-dimensional coating flow of a viscoelastic fluid film on a substrate of arbitrary shape. *Journal of Non-Newtonian Fluid Mechanics* 2001; **95**:199.
26. Gorla RR, Byrd LW. Effect of electrostatic field on film rupture. *ASME Journal of Fluid Engineering* 1999; **121**:651.
27. Ellen CH, Tu CV. An analysis of jet stripping of liquid coatings. *Journal of Fluids Engineering* 1984; **106**:399.
28. Tuck EO, Vanden Broeck JM. Influence of surface tension on jet stripped continuous coating of sheet materials. *A.I.Ch.E Journal* 1984; **30**:808.
29. Moriarty JA, Schwartz LW, Tuck EO. Unsteady spreading of thin liquid films with small surface tension. *Physics of Fluids A* 1991; **3**:733.
30. Kalliadasis S, Bielarz C, Homsy GM. Steady free-surface thin film flows over topography. *Physics of Fluids* 2000; **12**:1889.
31. Stillwagon LE, Larson RG. Fundamentals of topographic substrate leveling. *Journal of Applied Physics* 1988; **63**:5251.
32. Stillwagon LE, Larson RG. Leveling of thin films over uneven substrates during spin coating. *Physics of Fluids A* 1990; **2**:1937.
33. Rushak KJ, Weinstein SJ. Viscous thin-film flow over a rounded crested weir. *ASME Journal of Fluid Engineering* 1999; **121**:673.
34. Wilson SK, Duffy BR. On the gravity-driven draining of a rivulet of viscous fluid down a slowly varying substrate with variation transverse to the direction of flow. *Physics of Fluids* 1998; **10**:13.
35. Burelbach JP, Bankoff SG, Davis SH. Nonlinear stability of evaporating/condensing liquid films. *Journal of Fluid Mechanics* 1988; **195**:463.

36. Wilson SK, Davis SH, Bankokff SG. The unsteady expansion and contraction of a long two-dimensional vapor bubble between superheated or subcooled parallel plates. *Journal of Fluid Mechanics* 1999; **391**:1.
37. Pumir A, Manneville P, Pomeau Y. On solitary wave running down on an inclined plane. *Journal of Fluid Mechanics* 1983; **135**:27.
38. Takeshi O. Surface equation of falling film flows with moderate Reynolds number and large but finite Weber number. *Physics of Fluids* 1999; **11**:3247.
39. Quéré D. Fluid coating on a fiber. *Annual Review of Fluid Mechanics* 1999; **31**:347.
40. Tuck EO, Bentwich M. Sliding sheets: lubrication with comparable viscous and inertia forces. Journal of Fluid Mechanics 1983; **135**:51.
41. Khayat RE, Welke S. Influence of inertia, gravity, and substrate topography on the two-dimensional transient coating flow of a thin Newtonian fluid. *Physics of Fluids* 2001; **13**:355.
42. Benney DJ. Long waves in liquid films. *Journal of Mathematical Physics* 1966; **45**:150.
43. Salamon TR, Armstrong RC, Brown RA. Traveling waves on vertical films: Numerical analysis using the finite-element method. *Physics of Fluids* 1994; **6**:2202.
44. Shkadov VY. Wave conditions of a flow in a thin viscous layer under the action of gravitational forces. *Izvestiya Akademii Nank SSSR Mekhanika Zhidkosti i Gaza* 1967; **1**:43.
45. Wilkes JO, Nedderman RM. The measurement of velocities in thin film of liquid. *Chemical Engineering Science* 1962; **17**:177.
46. Bertschy JR, Chin RW, Abernathy FH. High-strain-rate free-surface boundary-layer flows. *Journal of Fluid Mechanics* 1993; **126**:443.
47. Khayat RE. Transient free-surface flow inside thin cavities of viscoelastic fluids. *Journal of Non-Newtonian Fluid Mechanics* 2000; **91**:15.
48. Zienkievicz OC, Heinrich JC. A unified treatment of steady-state shallow water and two-dimensional Navier–Stokes equations—finite-element penalty function approach. *Computer Methods in Applied Mechanics and Engineering* 1979; **17/18**:673.
49. Sell GR, Foias C, Temam R. *Turbulence in Fluid Flows*: *A Dynamical Systems Approach*. Springer: Berlin, 1993.
50. Deane AE, Kevrekidis IG, Karniadakis GE, Orszag SA. Low-dimensional models for complex geometry flows: application to grooved channels and circular cylinders. *Physics of Fluids A* 1991; **3**:2337.
51. Holmes P, Lumley JL, Berkooz G. *Turbulence*, *Coherent Structures*, *Dynamical Systems and Symmetry*. Cambridge University Press: Cambridge, 1996.
52. Khayat RE. Finite-amplitude Taylor-vortex flow of viscoelastic fluids. *Journal of Fluid Mechanics* 1999; **400**:33.
53. Ashrafi N, Khayat RE. A low-dimensional approach to nonlinear plane-Couette flow of viscoelastic fluids. *Physics of Fluids* 2000; **12**:345.
54. Kriegsmann JJ, Miksis MJ, Vanden-Broek J. Pressure driven disturbances on a thin viscous film. *Physics of Fluids* 1998; **10**:1249.
55. Hamerock BJ. *Fundamentals of Fluid Flow Lubrication*. McGraw-Hill: New York, 1994.
56. Middleman S. *Modeling Axisymmetric Flows*. Academic Press: San Diego, 1995.
57. Plateau J. *Statique Expérimentale et Théorique des Liquids Soumis aux Seules Forces Moléculaires*. Gauthier-Villars: Paris, 1973.
58. Frenkel AL, Babchin AJ, Shlang LT, Sivashinsky GI. Annular flows can keep unstable films from breakup: nonlinear saturation of capillary instability. *Journal of Colloid and Interface Science* 1987; **115**:225.
59. Frenkel AL. On evolution equations for thin films flowing down solid surfaces. *Physics of Fluids A* 1993; **5**:2342.
60. Chandrasekhar S. *Hydrodynamic and Hydromagnetic Stability*. Dover: New York, 1961.

